Studia Geotechnica et Mechanica, Vol. XXVI, No. 3–4, 2004

INFLUENCE OF LIVE LOADS ON THE SOIL–STEEL BRIDGES

CZESŁAW MACHELSKI

Bridge Division, Civil Engineering Institute, Wrocław University of Technology,
Wybrzeże Wyspiańskiego 27, 50-370 Wrocław, Poland,
tel.fax. (+48) 71 320-27-48, e-mail: czesław.machelski@pwr.wroc.pl

GRZEGORZ ANTONISZYN

Bridge Division, Civil Engineering Institute, Wrocław University of Technology,
Wybrzeże Wyspiańskiego 27, 50-370 Wrocław, Poland,
tel. (+48) 71 342-72-46, e-mail: grzegorz.antoniszyn@pwr.wroc.pl

Streszczenie: Przedstawiono wyniki analiz sił wewnętrznych i przemieszczeń w podatnych konstrukcjach gruntowo-powłokowych. Na podstawie wyników badań na obiekcie rzeczywistym wykazano, że ugięcia powłoki pod obciążeniem krótkotrwałym (zmiennym) są analogiczne do ugięć w mostach belkowych wykonanych z betonu zbrojonego lub sprężonego. Umożliwia to zarówno traktowanie analizowanych konstrukcji jak układów liniowo-sprężystych, jak i tworzenie dla nich funkcji wpływu sił wewnętrznych w powłoce. Wyniki badań wykorzystano do utworzenia modelu fizycznego (numerycznego) mostu. Wykazano również, że pod obciążeniem długotrwałym warstwa kontaktowa (grunt w styku z powłoką) przystosowuje się do działania tego obciążenia. W wyniku tego ulegają zmianie (w funkcji czasu) wartości sił wewnętrznych.

Abstract: The results of analysis of internal forces and displacements in flexible soil–steel structures are presented. Based on the results of in-situ tests of the bridge it is shown that the deflections of the shell subject to short-term load (live load) are analogous to the displacements of reinforced or prestressed concrete bridges. This feature allows considering the analysed structure as linearly elastic system and using the concept of influence function of internal forces for the analysis of shell. The results of in-situ research were utilized to develop a physical (numerical) model of bridge. It is also shown that under a long-term load the contact layer (the interface between soil and steel shell) adapts to the load. As a result, the values of internal forces change in the function of time.

Rezume:

1. INTRODUCTION

Such engineering structures as bridges, culverts, tunnels, pedestrian subways and viaducts made from steel shell and a soil backfill surrounding it are soil–steel structures. They are constructed in such a way as to take an advantage of composite interaction between those two load-carrying elements. An example of the soil–steel structural plate system is shown in figure 1.

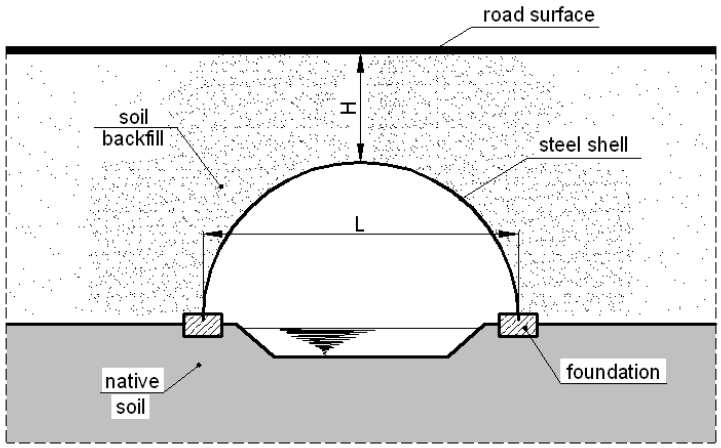

Fig. 1. Components of soil–steel structure

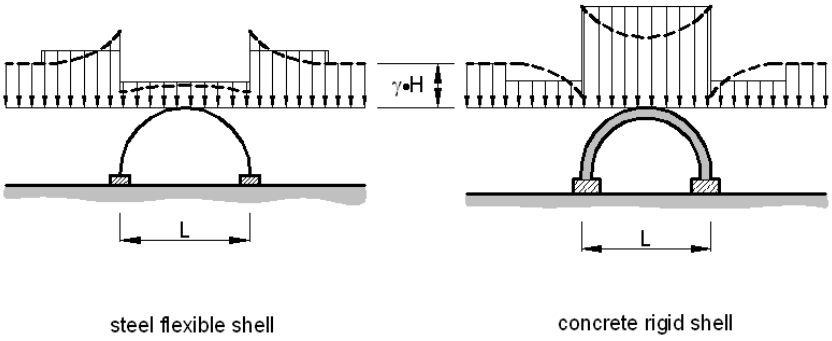

Fig. 2. The load of the shell, depending on its rigidity

The force the earth pressure exerts on the structure depends on the stiffness of shell with respect to the surrounding soil backfill [11]. For that reason, the soil–steel structures are mainly divided into two groups: rigid and flexible. The rigid structures are considered to be massive ones, made from the low-tensile strength materials, such as: concrete,

stone or brick. On the other hand, the flexible structures are load-carrying structures (shells) made from steel or aluminium or even plastic corrugated plate. The characteristic distributions of earth pressure exerted on both types of shells are presented in figure 2 (where $\gamma \cdot H$ is the earth pressure in a horizontal plane above the shell). This explains the necessity of applying two different approaches when dealing with flexible and rigid shells. The flexible structures are under consideration in the present work.

The history of application of the flexible steel shell structures in bridge engineering is dated back to the end of the nineteenth century [8], [11], [15], [19]. Initially, such bridge structures were constructed as riveted pipes with circular cross-section and a relatively short span L. The second generation of that type of structures had a span in the range of 8–16 m. Their development was ensued in Canada in the 60's if the twentieth century [1], [11]. It was encouraged by a better understanding of principles of interaction of soil and steel shell. In that period, an intensive research in these structures resulted in the development of a number of analytical methods for determining the distribution of internal forces and stresses in structure. The progress in computational methods based on FEM [1], [6], [11], [15] contributed to development of the third generation of soil–steel structures which were characterized by: a) span being longer than 16 m, b) a further introduction of the box section profiles to span of up to 8 m and c) utilization of techniques combining different materials [16], i.e. longitudinal and transverse stiffening ribs (corrugated steel plate with reinforced concrete) and reinforced soil (soil and geotextiles) and cement or lime stabilized soil. In the 90's of the twentieth century, the corrugated plates with large corrugation (380·140 mm and 400·150 mm) were introduced to bridge engineering which enabled us to construct the box section structures significantly exceeding the span length of 12 m at the overburden depth of 0.45–1.5 m [19]. Nowadays, the range of application of flexible soil–steel structures covers not only the building of new structures but also the strengthening of existing ones.

A proper interaction between soil and steel corrugated plate requires a good quality aggregate and a proper compaction of backfill around the steel plate [8]. As has been learned from the experience of installation of such structures, sands, river gravel, sand–gravel mixtures, and coarse-grained ones, whose fraction ranges from 0 to 32 (45) mm, are suitable for compaction at any weather conditions. The cases of using the light aggregates as backfilling are also known. It is especially advantageous during the installation of structures with high embankment on a soft subsoil (weak soil).

The flexible structures, owing to the interaction of the steel structural plate with the surrounding soil, are able to carry a very large loading taking advantage of arching [21]. That phenomenon is observed as a reduction of soil pressure on the top surface of shell (even as much as 70%). Arching is the phenomenon of redistribution of loading of a shell as a result of the occurrence of tangent stresses, which counteract the displacements in soil mass as in shown in figure 3. The shell tries to decrease its rise

due to vertical loads, simultaneously increasing its horizontal dimension. The displacement of the shell in horizontal direction is responsible for the resistance of soil which next reduces the possibility of increasing its horizontal dimension and thereby a decrease in its rise. This situation favourably affects the bearing capacity of the whole system.

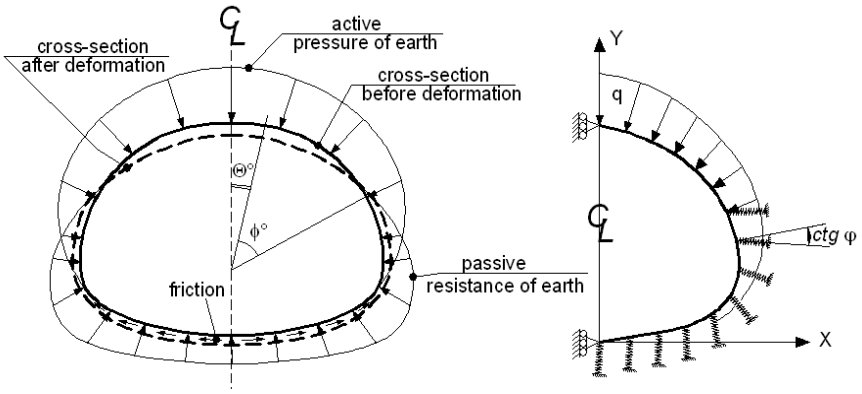

Fig. 3. Model of soil–steel structure proposed by Klöppel and Glock

The previous theories explaining the arching phenomena [21] have been initiated by Forchheimer in 1882 and next by Engesser (1882), Bierbaumer (1913), Voellmy (1937), Terzaghi (1943), Finn (1963), Luscher and Hoeg (1963), Protodyankonov (1966), Nielson (1967), Caquot and Kerisel (1967), Davis (1968). The most valuable is theory derived by Terzaghi [21]. The analytical methods of Martson–Spangler (1960) considered mainly the small culverts with circular section [1], [21]. In the ring compression theory of White and Layer (1960), they proposed to consider the side walls as being subject to a uniform ring compression [11]. The above-mentioned assumptions are confirmed by the results of observations made for the case when the depth of overburden does not exceed 1/8 of the shell diameter. The theory of Klöppel and Glock (1970) [1] is based on the model of plane frame shown in figure 3. Soil affects the walls of shell by elastic elements, which can carry only axial loads.

In the 80's of the twentieth century, the design standards and guidelines for dimensioning the structures have been developed in the United States of America and in Canada. In American standards AISI (1984) and AASHTO (1983) [21], one general formula for determining the maximal axial force in the flexible shell taking into account the radius of curvature of arch R_T was introduced

$$N = \gamma \cdot H \cdot R_T \,. \tag{1}$$

According to OHBDC (Ontario Highway Bridge Design Code, 1983) [18] a the maximum axial thrust in the shell wall yields

$$N = \mu_1 \cdot (\gamma \cdot H \cdot R_T) \,. \tag{2}$$

The coefficient of arching μ_1 dependent on the depth of overburden and the shape of shell is shown in figure 4.

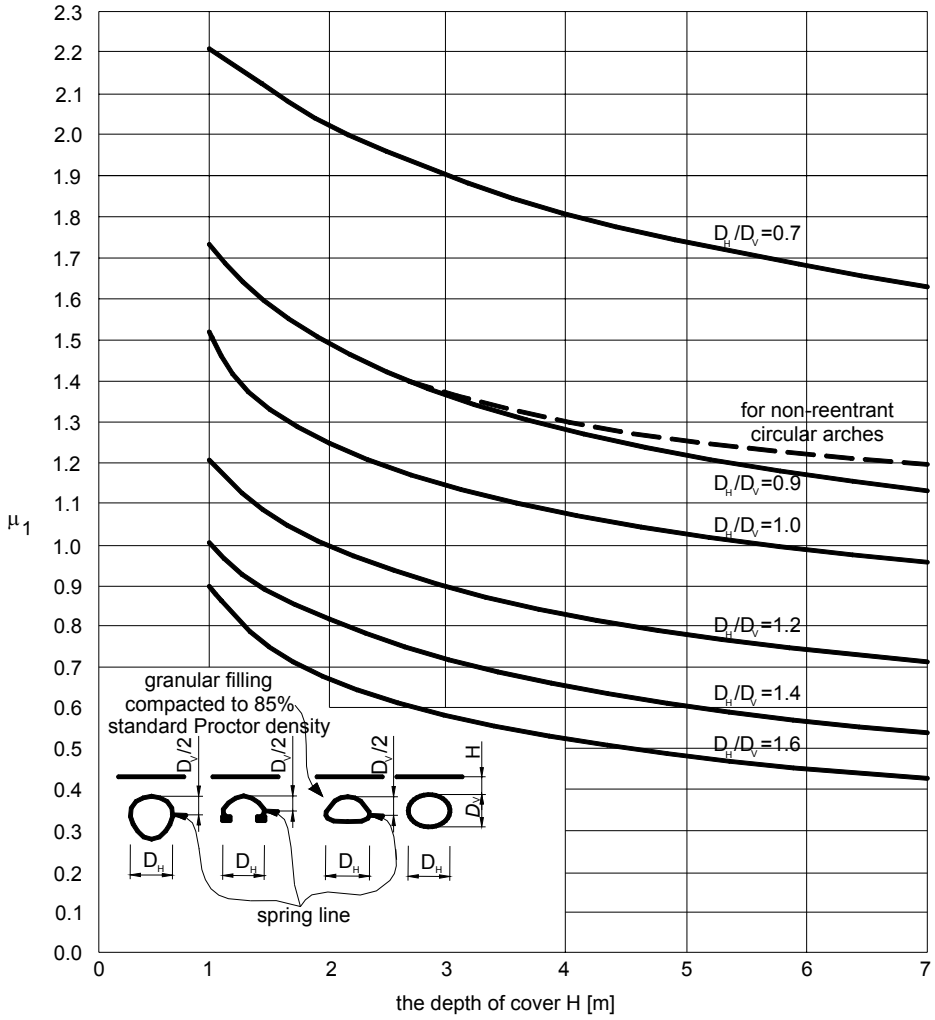

Fig. 4. Coefficient μ_1 according to OHBDC

The SCI method (Soil–Culvert Interaction, 1983) was developed by DUNCAN [21]. Devising of this method lasted for a few years because it was based on the results obtained from the observation of already built structures tested in a real scale. These results and numerical simulations (FEM) complemented each other successfully. To

the calculation procedures Duncan has introduced a nonlinear relation between stresses and displacements that concern the backfill around the structural plate (the so-called Duncan's soil model).

Because of their complex character the soil–steel structures present a tough problem to solve. Designing of three-dimensional numerical model [5], [6], [16] is inconvenient and tedious and that is why most of software programs developed for carrying out the analysis of such structures reduce the problem to two dimensions (figure 3), based on the plain strain assumption. The first computer program used in such an analysis was CANDE (Culvert ANalyses and DEsign Program) designed by Katona and Smith in 1976. Nowadays in order to model the soil–steel structures, a number of programs based on FEM, for example COSMOS, ROBOT, SPIDA, NLSSIP, etc., are used.

In current models of soil medium interacting with the structure, one takes into account an elastic-plastic behaviour of soil [9], [17], which more precisely describes the arching phenomena. For that purpose computer programmes, based on FEM, such as CRISP'92, HYDROGEO, Z-SOIL, PLAXIS, ABAQUS, ANSYS should be used. Equally important is the issue of modelling a contact zone between soil medium and the structure. In that case, special finite elements characterized by complex physical parameters such as shear module and compressibility module with non-linear force–displacement relation are usually used. The contact layer at the contact of two media, called popularly *interface*, is commonly used also for modelling the connections of steel elements, for example in glue joints. The parameters of contact layer are adjusted to a specific situation, i.e. to characteristics of soil medium (dampness, cohesion), the stiffness of walls of structure, condition of contact surface (roughness), time duration of live loads.

2. THE DISTRIBUTION OF ROAD LOAD ALONG A SHELL

The essential feature of load distribution through the roadway surface and the soil backfill is the ratio of dimensions of the horizontal projection of a structure

$$\beta = \frac{B}{L} \tag{3}$$

and the depth of a structure at the crown point

$$\vartheta = \frac{h_z + f}{L}, \tag{4}$$

where:

B – the width of a bridge structure (taken as a section perpendicular to the road axis),

L – span, i.e. the distance between the points of support,

$h_z + f$ – the sum of the depth of soil backfill and the depth of corrugation of structural plate.

This study considers the bridge systems characterized by the similar values of B and L. The structures with a large width B, several times exceeding its span L, are usually constructed as box-shaped (pipes) with a variety of cross-section shapes. They require distinct approach. In bridges with a low construction depth (a small depth of backfill), the development of local effects, unfavourable for such a type of structure [12], is usually observed. The presented results of analysis are related to the structures with the depth of backfill at the crown point in the range of $0.08 < \vartheta < 0.20$. The results of test measurements for the structure, which meets those requirements, are given below. The geometrical parameters of the structure tested [4], [10] are:

- bridge span L = 12.315 m;
- width of roadway B_j = 7.00 m;
- width of bridge B = 11.40 m;
- depth of backfill, including road surface, at the crown of point, h_z = 1.35 m.

Load-bearing element of the structure is a corrugated plate *Super Cor SC-56B* with the thickness t = 7 mm and the length of corrugation (pitch) a = 380 mm and its depth f = 140 mm. In the middle part of the span and at the corners, the cover plates made of the identical structural plate were applied. The steel sheets are connected by means of high-strength bolts [4]. The bridge has the shape of a circular frame in longitudinal section with two curvature radius at the corner R_n = 1.016 m and in the middle of the span R_s = 11.43 m.

The structural plate is founded in the concrete footing. The side walls of bridge are in the form of bevelled slopes with stone paving protection facing, which protects the soil backfill under the road surface (figure 5).

To identify structural performance of the bridge after two years of its service, five loading schemes of single vehicle of LIAZ type of a total weight of 400 kN and the following axle thrusts were applied:

$$P_1 = 55.4 \text{ kN} \ (a_{12} = 3.50 \text{ m}), \quad P_2 = 93.8 \text{ kN} \ (a_{23} = 2.60 \text{ m}), \quad P_3 = 122.2 \text{ kN},$$

$$(a_{34} = 1.35 \text{ m}), \quad P_4 = 82.4 \text{ kN} \quad (a_{45} = 1.35 \text{ m}), \quad \mathrm{P}_5 = 46.2 \text{ kN},$$

where:

$P_1, \ldots, P_5$ – the burden of the consecutive vehicle's axles, being counted starting from the vehicle's front;

$a_{12}, \ldots, a_{45}$ – the distance between the wheel axles of vehicle.

In figure 5, the location of vehicle and the arrangement of its wheels on the roadway during the bridge test are given. The location of the vehicle on the bridge roadway at the others schemes differs only in the arrangement of vehicle at the cross-section (figure 6). The static loading tests included two groups of loading using a single vehicle:

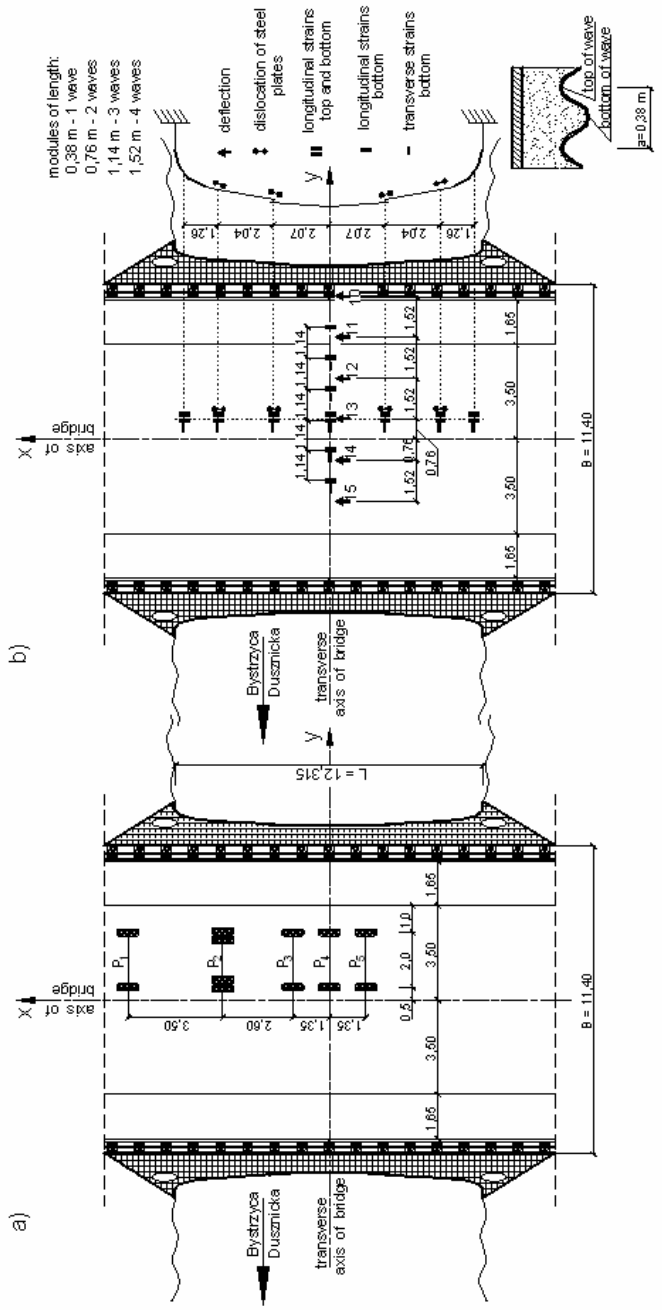

Fig. 5. Position of vehicle on the roadway of bridge in the loading scheme S-I and positioning of sensors (measuring devices)

- long lasting, for central position of the vehicle (schemes S-I and S-V);
- short lasting, for the vehicle which has been driving along the line parallel to the roadway axis, taking into account its temporary pulling off in order to register measurement outcomes (schemes S-II, S-III and S-IV).

The measurement basis shown in figure 5 was established for three groups of geometrical quantities under consideration:

- deflection in the middle of the span;
- reciprocal displacement (dislocation) at the contact of steel sheets in chosen areas of the span;
- unit strains in the circumferential direction (along the line of corrugation of steel plate ε_x) and lateral direction (perpendicular to circumferential ε_y) on the bottom surface of sheet.

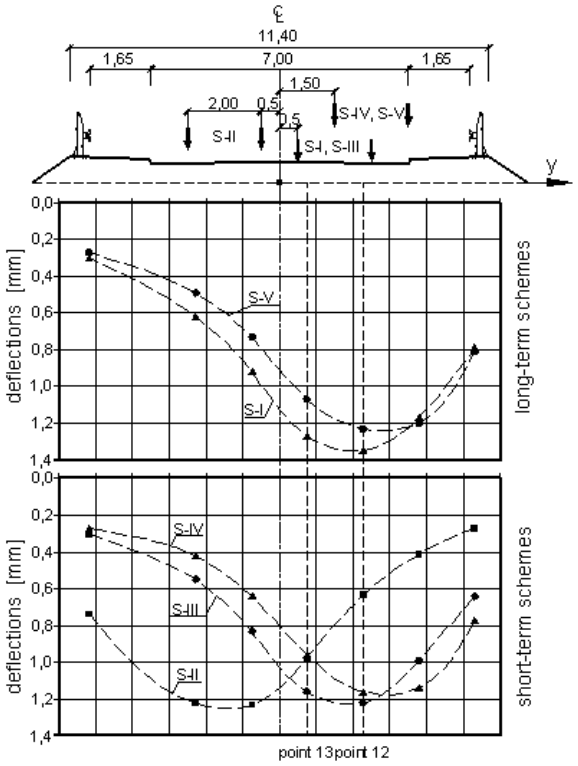

Fig. 6. Deflections in the loading schemes analysed

In figure 6, the plots representing deflection obtained from the in-situ measurement for the middle span section of shell are presented. At the top of figure 6 the position of vehicle in the cross-section of bridge is given. Based on the displacements shown in

figure 6 it can be concluded that the freedom of shell displacement in the zone of slopes is noticeable (the lack of clamping). The local deformation of shell under the wheels of vehicle has not been observed either, as it usually takes place in the case of structures with low construction depth [12].

In figure 6, a dashed line joints the points representing measurement results.

3. INTERACTION OF SOIL BACKFILL AND STEEL STRUCTURE

3.1. DEFLECTIONS

In the evaluation of measurement results, their stability in function of time t is of essential importance. The curve representing characteristic changes in the deflection is shown in figure 7. At the instant t_p we record an initial reading under full loading of bridge (point P). Its intensity and position do not change untill the time t_k which is the end of loading process (point K). At the instant t_r there is not any live loading on the bridge (point R). After the time t_r the structure is unloaded which means that it undergoes the stress relief. The residual forces in the members of structure, which have developed during the loading process, decrease and thereby the displacement that has increased in the time interval $<t_p, t_k>$ is now reduced.

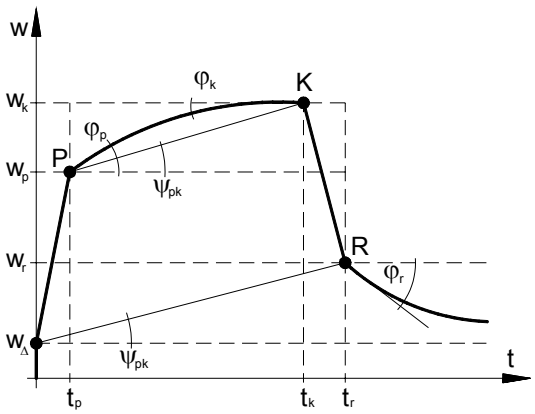

Fig. 7. Changes of deflection in the function of time

The symbols $w(t)$ the φ_p and φ_k in figure 7 stand for the momentary velocity changes of deflection treated as the tangents to the curve of displacement

$$\varphi = \frac{dw}{dt}. \tag{5}$$

For the engineering structures, the relationship $\varphi_p > \varphi_k$ holds. Usually we have $\varphi_k \to 0$ (which has happened in the case of realization of schemes S-I and S-V). The value of ψ_{pk} is in this case an average speed of the change in displacement. The parameters given above are the delayed strain ratios, which are encountered in the case of ideally elastic structures:

$$\psi_{pk} = \frac{w_k - w_p}{t_k - t_p} . \tag{6}$$

Based on the results given in the table one can compare the values obtained in the primary scheme of loading of bridge (S-I) with the secondary one (S-V). The values ρ_{pk} show relatively small influence of delayed effects on the structure deformation. The values of this coefficient are analogous to those being usually obtained, for example, for the reinforced concrete bridges.

Table

Comparison of scheme S-I with scheme S-V

The quantity analysed	Scheme S-I		Scheme S-V	
	Point 12	Point 13	Point 12	Point 13
w_p [mm]	1.12	1.05	1.12	0.96
w_k [mm]	1.35	1.27	1.23	1.07
w_r [mm]	0.27	0.25	0.08	0.09
ψ_{pk} [mm/min]	0.00575	0.00550	0.00367	0.00367
φ_p [mm/min]	0.0180	0.0180	0.0167	0.0133
w_Δ [mm]	0.040	0.030	-0.030	-0.040
$\rho_{pk} = (w_k - w_p)/w_k$	0.1704	0.1732	0.0894	0.1028
$\rho_r = w_r/w_k$	0.2000	0.1970	0.0650	0.0841

The deflections w_r that remain in the structure after its unloading are expressed by the rate ρ_r. They are indicative of irreversible effects. The values of displacements connected with that phenomenon can be estimated in the form of deflection w_Δ (figure 7),

$$w_\Delta = w_r - \psi_{pk} \cdot t_r . \tag{7}$$

In such a case, the change of the sign of deflection coefficient seems to be interesting

$w_\Delta > 0$ for the primary loading,

$w_\Delta < 0$ for the secondary loading.

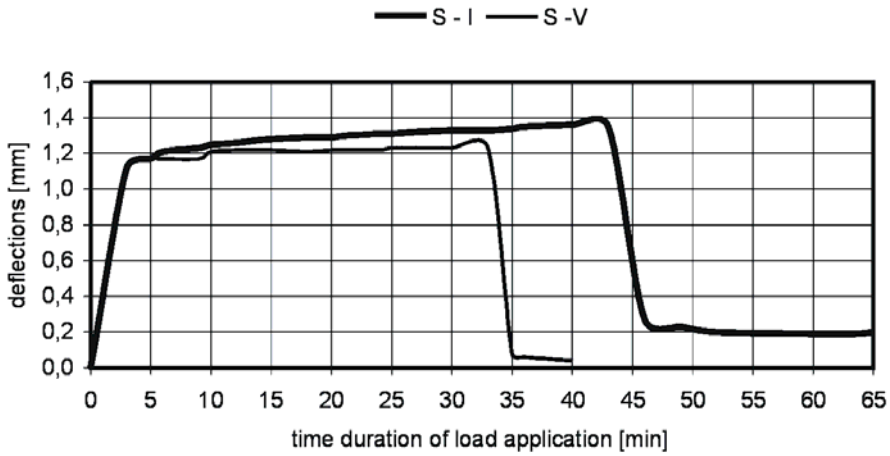

Fig. 8. Changes of deflection of point 12 during the time of long-term load application

In figure 8, there is given the deflection of point 12 in the function of time, while in table 1 there are presented the calculated characteristics obtained during in-situ tests for the load schemes S-I and S-V. In the case of a short-term loading (schemes S-II, S-III and S-IV) and the load traversing the span of the bridge, the deflections w_r are within the range of values given in the table.

3.2. UNIT STRAINS

The curves representing unit strains in the circumferential strip of shell situated close to the line of vehicle's wheels ($y = 0.76$ m from the longitudinal axis of bridge, as in figure 5) shown in figures 9 and 10. Those curves are divided into three groups: those representing the results obtained directly after loading the deck with vehicle (initial), those just before removing the loading vehicle from the bridge (final) and those representing the values remained in the shell after pulling away the load (residual). Each of those graphs represents the unit strains in the circumferential direction ε_x for the pair of points situated on one corrugation of plate, the lowest ε_d and the highest ε_g. The unit strains were measured at the lowest and the highest points of grid, accessible from below. In the central parts of curves, the location of vehicle in respect of the length of bridge is shown (the position of vehicle with respect to cross-section of bridge is shown in figure 6).

The couples of curves of unit stresses enable mapping the changes in internal forces, i.e. bending moments and axial forces, along the circumferential strip of the structure. On the basis of the difference in unit strains

$$\Delta\varepsilon = \varepsilon_g - \varepsilon_d \tag{8}$$

the values of bending moments in the circumferential strip of shell can be estimated

$$m_x = \frac{EI}{h-t}(\varepsilon_g - \varepsilon_d)\,, \tag{9}$$

where:

E –Young's modulus of steel,

I – the moment of inertia of the width a of the strip being analysed,

$f = h - t$ – the amplitude of corrugation for the overall depth h of plate and the thickness t.

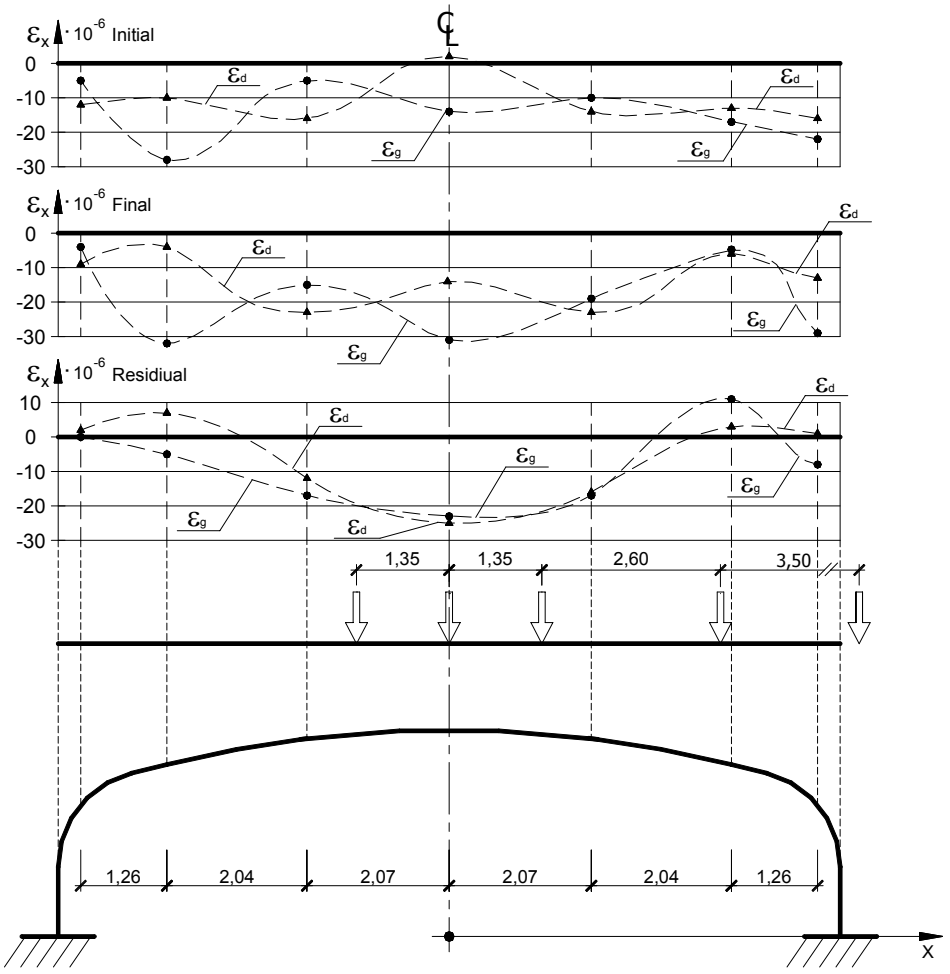

Fig. 9. Unit strains in circumferential strip in loading scheme S-I

The sign of $\Delta\varepsilon$ gives the information on the direction of the moment m_x. In the case where the change of sign of $\Delta\varepsilon$ is repeated many times, as in figures 9 and 10, the

change of bending along the length of circumferential strip is also seen. On the other hand, when ε_g and ε_d in the same cross-section have the same sign, this means that there exists an eccentric compression ($\varepsilon < 0$) and a resultant axial force is localized in the core of the section. A middle area of the span in an initial period of load application and the corners of the structure after the vehicle is off the structure (figure 9) are exceptions to the above observation. Very small (or zero) values of $\Delta\varepsilon$ show that the section is under axial compression. They appear in the areas of the change of direction of moments and in the case of residual deformations. The frame corners, particularly during the primary loading (scheme S-I), are exceptions to that. The characteristics of the effects of live loads given above testify to the similarity in structural behaviour of the bridges tested and the vaulted bridges (brick, stone, concrete). A smaller depth of a soil backfill above the shell is responsible for the change in these static characteristics that are appropriate for the frame construction bridges [12].

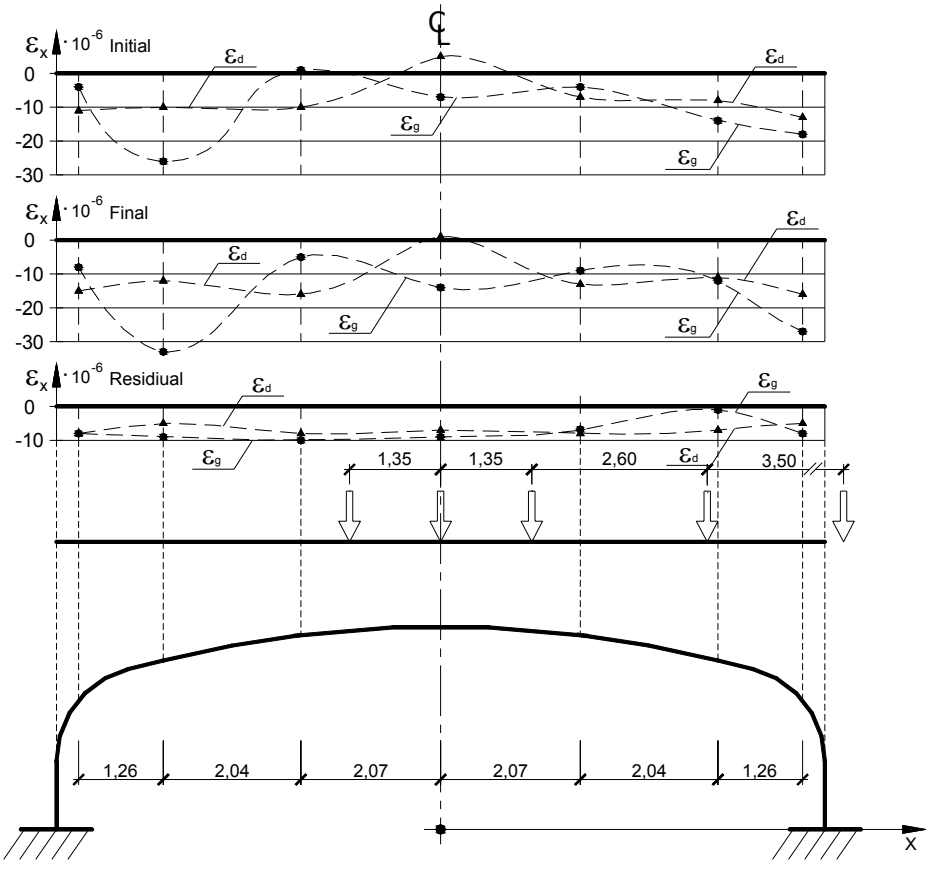

Fig. 10. Unit strains in circumferential strip in loading scheme S-V

An average value of the unit strains is considered to be an equally important information obtained from the shape of curves

$$\varepsilon_{\text{avg}} = \frac{\varepsilon_g + \varepsilon_d}{2} . \tag{10}$$

The line determined for ε_{avg} gives information on the change of the value of axial force estimated as follows:

$$n_x = \frac{Fh}{2(h-t)}\left[\varepsilon_g + \varepsilon_d(1-2\frac{t}{h})\right] \approx \frac{F(\varepsilon_g + \varepsilon_d)}{2} , \tag{11}$$

where F is an area of the section separated from the strip of shell.

The curves in figure 9 show that directly after the load application, the maximum values of axial forces are developed at the corner area, and the minimum values – at the crown point. Then the axial forces along the length of the strip are being stabilized until they reach comparatively equal values. The substantial values of n_x (compression) are measured after the unloading of roadway, while at the corner they are rather small and have an inverse sign (tension). The changes of unit strains during the measurement are depicted in figure 11.

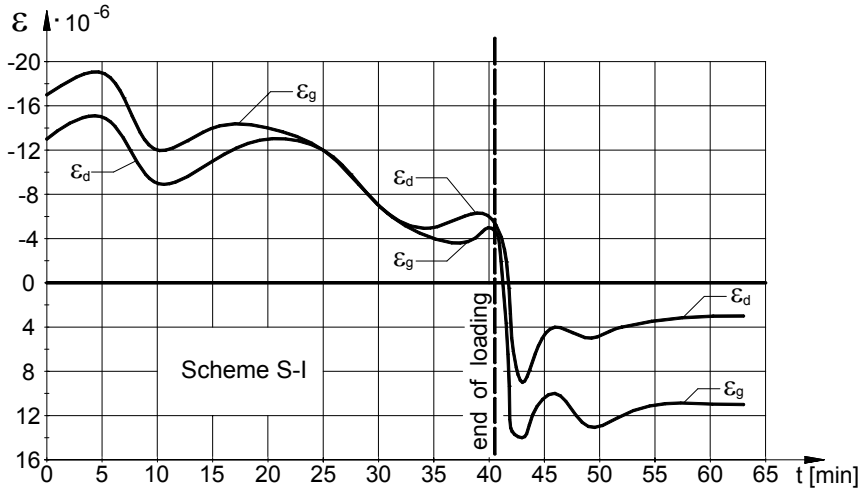

Fig. 11. Change of unit strains at the cross-section of corrugation (x = 4.11 m, y = 0.76 m)

In the case of the primary loading of structure (scheme S-I), the change of sign of ε after loading removal from the bridge was observed. This proves that in the contact zone, exactly at the moment of loading, the soil forced the unit strain of the shell on the level of ε_g equal to $16 \cdot 10^{-6}$ and then adapted itself to this state (with loading) at

$\varepsilon_g = -5 \cdot 10^{-6}$. When the load was removed from the bridge, the opposite situation took place – the change of direction of mutual interactions between soil and shell, hence $\varepsilon_g = 10 \cdot 10^{-6}$. That phenomenon shows that the internal forces of soil–steel system subject to long-term loads can be redistributed approaching a natural configuration in which they reach their minimum values at the interface. The phenomenon presented in figure 11 also occurred at the other point tested (figure 12). In this case, after the load removal from the bridge, only the change of sign of bending moment appeared (but not the change of axial force, as in figure 11).

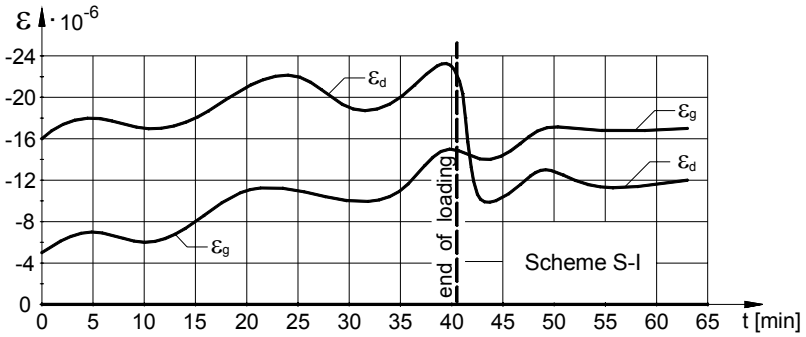

Fig. 12. Change of unit strains at the cross-section of corrugation ($x = -2.07$ m, $y = 0.76$ m)

The results given in figure 11 testify to the inhomogeneity of system being comprised of the linearly elastic shell surrounded by loose (but compacted) soil medium. This inhomogeneity, a typical feature of soil–shell structure, is also emphasised in the case study of other bridge structure subject to live and pulsating load [13]. In this study, the measuring results at a current external loading were proven to be dependent on the actual deformation of shell which occurred before the test measurement. This phenomenon is also corroborated by the values $w_A < 0$ given in the table. Additionally, as it is proven in [13], the deflections of shell being subject to the static loading of road surface are also influenced by the vibration of soil medium.

In the case of secondary loading (scheme S-V), the value of n_x does not undergo any significant changes in comparison with the changes in initial and final states (figure 10). The residual strains emphasize the momentless state of strain and the value of axial force being constant along the length.

3.3. NORMAL STRESSES

Normal stresses for circumferential σ_x and transverse σ_y directions were calculated on the basis of the unit strains and at the same point, while the same stresses for the circumferential direction ε_x and for the orthogonal one ε_y using formulas

$$\sigma_x = \frac{E}{1-\nu^2} \cdot (\varepsilon_x + \nu \cdot \varepsilon_y) \tag{12}$$

and

$$\sigma_y = \frac{E}{1-\nu^2} \cdot (\varepsilon_y + \nu \cdot \varepsilon_x) \tag{13}$$

for E = 205000 MN/m^2 and ν = 0.30.

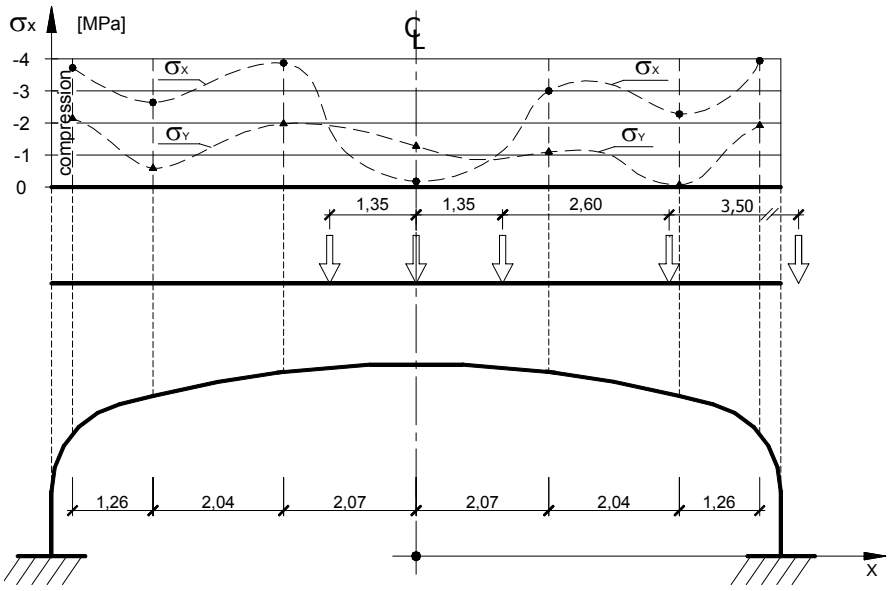

Fig. 13. Change of normal stresses in the circumferential strip during the long-term tests (scheme S-I)

In figure 13, there are shown the curves representing normal stresses for the bottom part of corrugation and circumferential line, the latter being at the distance of y = 0.76 m from the symmetry axis of the bridge (and also from the roadway). In the central part of figure 14, the position of vehicle's axis is given, and in its bottom part, a static scheme of circumferential strip is presented. The curves represent an initial stage of load application. The stress concentration due to a large change in the curvature of shell at corner is not observed here.

The results given in figure 14 are characterized by very small values of stresses (such small values only rarely appear in steel) under the service load that is similar to the half of standard load of class B [4]. The depth of backfill below the road surface is a main reason of this situation, since it ensures an effective distribution of load due to vehicle's wheels [10] and limits local deformations, which influence an increase in bending moments.

In figure 14, like in figure 13, the values of σ are shown, but calculated for the final stage of loading application.

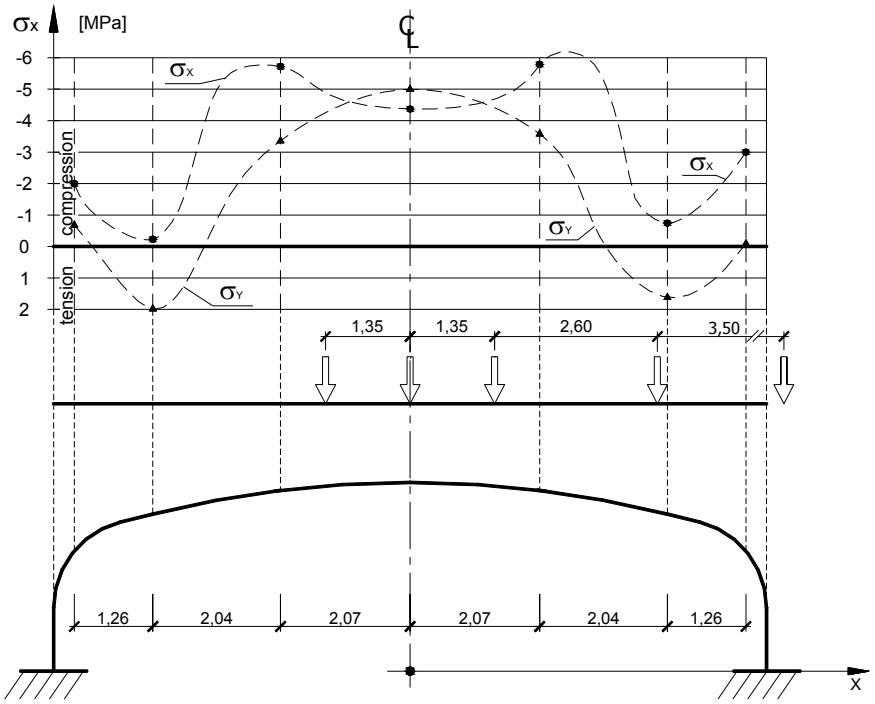

Fig. 14. Change of normal stresses in the circumferential strip during the long-term tests (scheme S-V)

3.4. THE INFLUENCE OF SERVICE TIME UPON THE BRIDGE

The results obtained from the load tests of the bridge, which had been carried out before it was opened for traffic [4], are compared to a similar load (ca. 95% in the case of deflection). It enables us to evaluate the change in a general stiffness of soil–steel structures as a result of service life [10]. In the case of deflections (results from figure 48 in [4] and the table)

$$\frac{w_{\text{old}}}{w_{\text{new}}} = \frac{3.06}{1.35} = 2.27\,. \tag{14}$$

In the case of unit strains (results from figure 44 in [4] and figure 12)

$$\frac{\varepsilon_{\text{old}}}{\varepsilon_{\text{new}}} = \frac{40 \cdot 10^{-6}}{23 \cdot 10^{-6}} = 1.74\,. \tag{15}$$

The result of comparison of the unit strains (15) at different vehicular loads is of significance for assessment purposes.

Additionally the results given above indicate that after a two-year period of service an increase in global stiffness of the structure, as in case analysed in [10], was obtained. This conclusion is supported by a direct comparison of the distribution of deflections in the cross-section (compare figure 48 in [4] for a single vehicle and, for example, figure 6).

4. COMPUTATIONAL MODELS

4.1. MODELS OF SHELL

A general model of bridge is presented in figure 15. The geometry of superstructure is represented in 3D space. The physical characteristics of elements were assumed to be linearly elastic. Fragments of the middle part of the structure are shown in figure 16a. Based on the results of numerical tests for chosen types of model of plate geometry covered with soil and on the results of in-situ survey, two models were accepted as the most effective, further being denoted as M1 and M2. They differ from

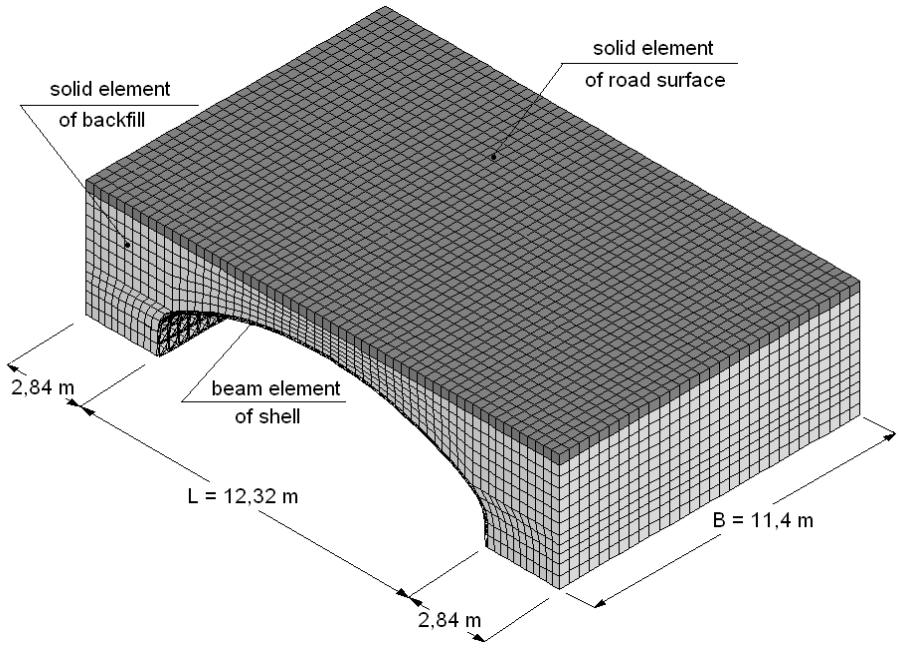

Fig. 15. General model of structural system

each other in the methods of mapping the geometry of corrugated plate. In both models, the soil backfill and road surface are modelled as isotropic continuum. The interface between the soil backfill and the steel structural plate (figure 16a) is modelled as spring elements of linearly elastic characteristics. Within their flexibility there are also included characteristics of soil medium (the angle of shearing resistance, dampness, cohesion), stiffness of structure walls, condition of contact surface (roughness), time of load application. In the discrete model, the characteristics of those elements are diversified all over the area of grid (figure 16a).

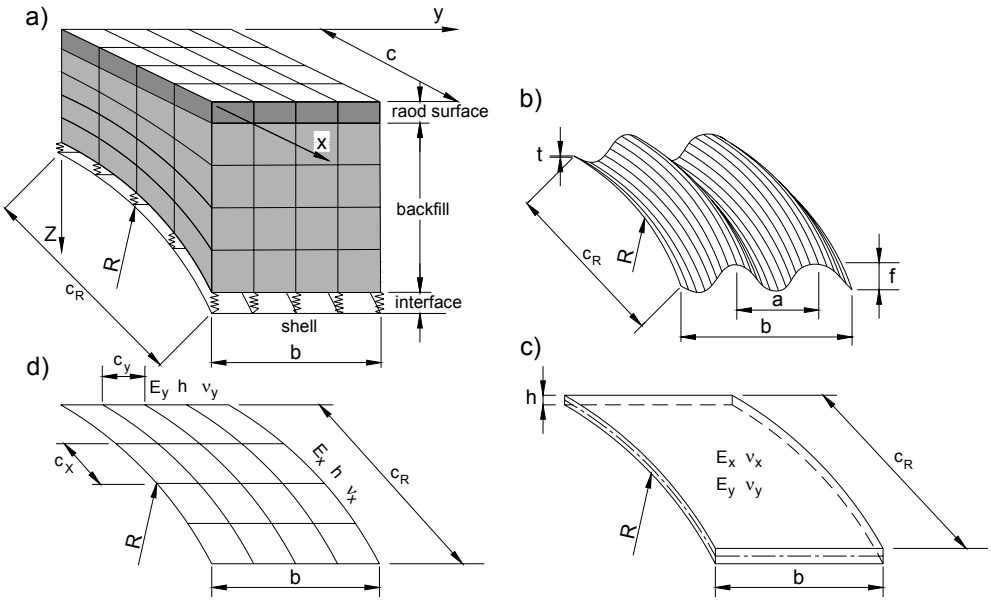

Fig. 16. Model M1 modelled with an orthotropic plate

The assumptions accepted for the model of interface concern the stationary and short-term loads which act on the surface of the road. Defining the functions that influence the internal forces in a shell is justified only for the model being characterized by the linear relationship of load–deflection. In the case of long-term loads, including also dead loads in the form of soil backfill, equipment of bridge and live loads which dynamically excite the bridge structure [13], it is advised to apply more complex and sophisticated models of interface.

In the model M1 (as in figure 16c) a corrugated plate is treated as orthotropic plate whose parameters are determined based on the equilibrium condition of stiffness of the separated plate fragment given in figure 16b. For the circumferential direction (x) one obtains the set of equations

$$\frac{EI_a}{a} = \frac{E_x h^3}{12}, \tag{16}$$

$$\frac{EA_a}{a} = E_x h, \tag{17}$$

and for transverse direction (y) one assumes the relationship

$$\frac{Et^3}{12} = \frac{E_y h^3}{12}. \tag{18}$$

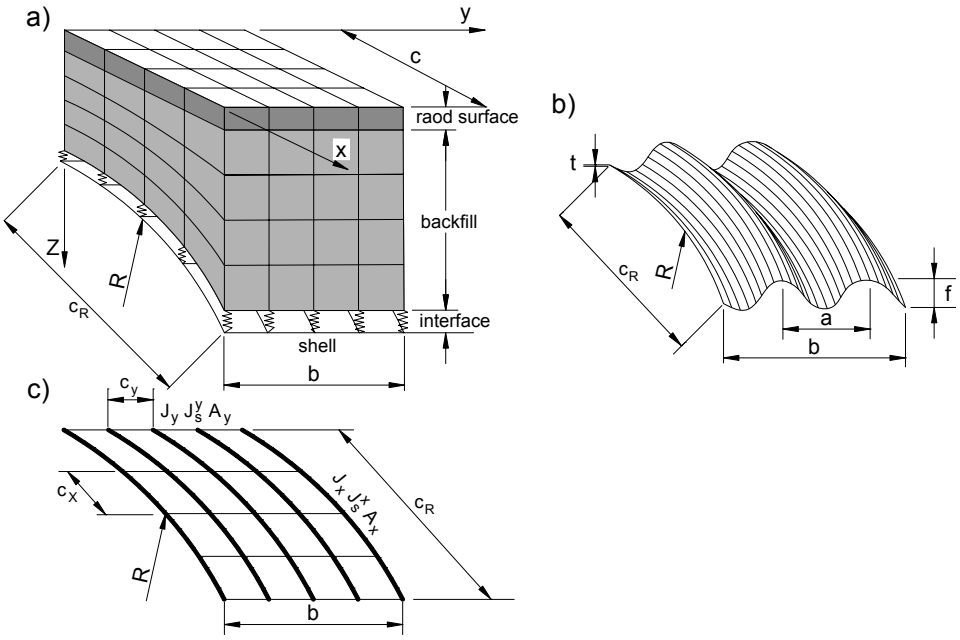

Fig. 17. Model M2 modelled with a beam grid

The values of the moment of inertia I_a/a and the area of cross-section A_a/a are related to the length of the corrugation a. A material characteristics of the shell, i.e. Young's modulus E = 205000 MN/m^2, is taken into account in the model. The Poisson coefficient of substitute orthotropic plate is estimated from the following relationship

$$\nu_x \cdot E_y = \nu_y \cdot E_x, \tag{19}$$

for example, for $\nu_x = \nu = 0.30$.

In the model M2 (figure 17c), the corrugated plate is modelled as the grid of beams consisting of the circumferential and transverse lines. The spans of nodes in the grid

are c_x and c_y. For such a model the geometrical characteristics of beams are determined in the following manner:

- for circumferential direction

$$A_x = A_a \frac{c_y}{a}, \tag{20}$$

$$I_x = I_a \frac{c_y}{a}; \tag{21}$$

- for transverse direction

$$A_y = \alpha_A \cdot c_x \cdot t, \tag{22}$$

$$I_y = \alpha_I \cdot c_x \frac{t^3}{12}. \tag{23}$$

The corrugation of plate in the form of the values of the coefficients α_A and α_I is taken into account. Neglecting the torsional stiffness GI_s^x and GI_s^y is advantageous owing to an interpretation of bending effects (at nodes), and particularly in the case of fine mesh and a large depth of soil backfill.

4.2. COMPARISON ANALYSIS

The bridge models were compared with a real-scale structure, which was subject to in-situ monitoring tests presented above. In both case, a numerical discretization of bridge models was carried out by means of SOLID isotropic volume elements that allowed modelling of the road surface whose material characteristics were as follows: E = 350 MPa and ν = 0.2. The soil backfill surrounding a structural corrugated plate was modelled by means of SOLID isotropic volume elements, which were given by the following material characteristics: E = 155 MPa and ν = 0.2 [2]. Geometrical characteristics of the corrugated plate of the SC 380·140·7 type, i.e. the plate depth t = 7 mm, the corrugation length a = 380 mm and the corrugation height f = 140 mm, are taken from the design guidelines laid down by ViaCon Poland company. They recommended $A_a/a = 3.73 \cdot 10^{-3}$ m^2/m and $I_a/a = 9.1826 \cdot 10^{-6}$ m^4/m. These values, i.e. the stiffness of corrugated plate with surface elements (figure 16c) and the beam elements (figure 17c), respectively, are expressed by formulas (16)–(23).

Numerical models of both structure and loading were modelled in FEM system COSMOS. In the models to be analysed, the following finite element types are chosen to model the shell:

- orthotropic surface elements SHELL4L for M1;
- beams BEAM3D with the spans $c_y = a$ = 38 cm and c_x = 30 cm for M2.

The loading due to vehicle wheels was distributed over the whole surface of its contact with the roadway surface of dimensions of 30×60 cm.

The results of numerical calculations are in accordance with in-situ measurement results in the range of deflection in the case of using both models M1 and M2. This is owing to the fact that the compatibility of deflections has been a fundamental condition of modelling a real-scale structure.

In the case of internal forces, and particularly stresses in model M1, the interpretation of results causes some difficulties. In terms of the above, the model M2 is more effective. But the results of stresses (unit strains) are significantly different from the corresponding ones measured in-situ.

The possibility of applying a linear elastic model is justified by the results of deflection obtained in the measurement tests presented in figure 8 and in the table. As a result of load application the instant values of deflections appear. Their increment is insignificant during the load application, and after the unloading constant deflections still are present. Such results are usually obtained for concrete and steel–concrete bridges whose design is usually based on linear elastic models. However, the results of measurements of unit strains and the normal stresses in the shell calculated on their basis show an enhancement of the effects connected with the function of time of load application and the condition of structure preceding the time of the tests. This phenomenon is illustrated by an example of the results given in figures 11 and 12. For those reasons, only short-term loads are considered in the paper. The influence functions of stresses which can be determined only in the case of linear model show the shape of the influence surface, i.e. the distribution of values of ordinates and their signs.

4.3. INFLUENCE SURFACES OF INTERNAL FORCES

An extremely important advantage of the model M2 lies in the possibility of creating the influence surface of internal forces and stresses indispensable for establishing the position of moving loads on the road surface of the bridge. To carry out those calculations, it is convenient to apply the kinematic displacement method in the form presented in [14]. In order to calculate the influence surface of axial force in any bar (for example, in circumferential strip shown in figure 17c), one assumes balanced forces (oppositely directed) at the nodes *ik* of the bar of the length l_{ik}

$$N_i = -N_k = \frac{EA_x}{l_{ik}}. \tag{24}$$

In the case of analysis of bending moments in the middle of the element *ik* of circumferential strip, the kinematic displacement is made by nodal bending moments

$$M_i = -M_k = \frac{EI_x}{l_{ik}}. \tag{25}$$

To create the influence surfaces of normal stresses at the bottom edge of corrugated plate it is necessary to apply both nodal forces in the modified form

$$N_i = -N_k = \frac{E}{l_{ik}} \tag{26}$$

and

$$M_i = -M_k = \frac{E}{l_{ik}} v_d\,, \tag{27}$$

where v_d is the distance of the bottom flange from the centre of gravity of section. Owing to the symmetry of cross-section of the shell it is sufficient to apply two kinematic displacements, which differ from each other in the direction of action of bending moment which determines the minimum and maximum values of normal stresses (compression) at the top and bottom edges of the shell (because $v_d = v_g = h/2$). In order to obtain the influence surface of tensile normal stresses, it is sufficient to attribute a reverse sign to the previously obtained surfaces.

As the result of loading the nodes with the imposed kinematic displacement presented above, one obtains the surface of displacement of nodes of roadway surface, which are simultaneously the ordinates of the influence surface of a static quantity under consideration. For instance, the vertical displacements (deflections) of road surface at the kinematic displacement given in (26) and (27) are ordinates of the influence surface of stress in the element *ik* being analysed, i.e. $w(x, y) = \xi(x, y)$. Thus, the ordinates of the influence surface should be interpreted according to the formula:

$$\sigma_{ik} = \zeta(x, y) \cdot P(x, y)\,, \tag{28}$$

where:

σ_{ik} – normal stress in the element *ik* being analysed, the element coordinates are x_0, y_0, and the stress depends on the concentrated force $P(x, y)$;

ζ – ordinate of the influence surface of stress at the point (x, y).

Normal stresses σ [MPa] are obtained when ζ is expressed in m^{-2}, and P – in MN.

An example of the influence surface of a normal stress σ_x at the top edge of structural plate at the point $F(x = 0.0$ and $y = 0.76$ m) is shown in figure 18. It is presented as the contour-line plan in the projection perpendicular to the surface of roadway. Negative values on ordinate denote compression. The following orientations (directions) of the figure are assumed:

- vertical, parallel to the axis of bridge (road surface);
- horizontal, parallel to the axis of physical obstacle.

Therefore the graph width is related to the model width (B = 11.40 m). In the figure height, the total length of bridge L_0 = 18.00 m with embankment (figure 15) is taken into account.

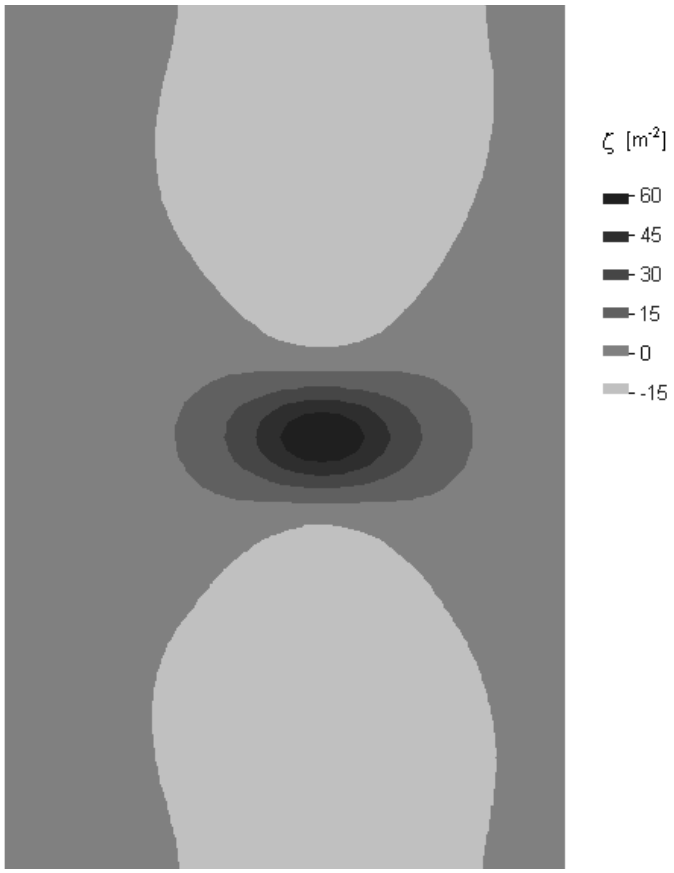

Fig. 18. Influence surface of normal stresses at the point (x_0 = 0, y_0 = 0.76 m) for circumferential strip (at the bottom of the steel corrugated plate)

The profiles of longitudinal and transverse contour plans given in figures 19 and 20 make a mapping of the shape of the influence surface of normal stresses σ_x easier. In this case (figure 19), there are also given the results for other points x (2.7; 4.2; 5.4 and 6.0) lying on the circumference of the strip being analysed (y = 0.76 m). In figure 20, the transverse profiles of those influence surfaces are shown, but at the points where the ordinates reach their maximum values.

The shapes of longitudinal profiles of the influence surface σ_x (figure 19) prove that the value of ζ takes different signs for the points lying in the mid span of the shell

strip. For that reason, in order to obtain σ_{max} it is indispensable to adjust the position of a live load to the shape and ordinates of contour-line plan. It is possible when a vehicle traverses the bridge along the axis of roadway, because in these circumstances the values of normal stresses would have alternate signs. For the points at the corners of frame, the values of ζ have the same sign. In that zone, the one-sign stresses (compression) due to a live load develop regardless of the position of load on the bridge.

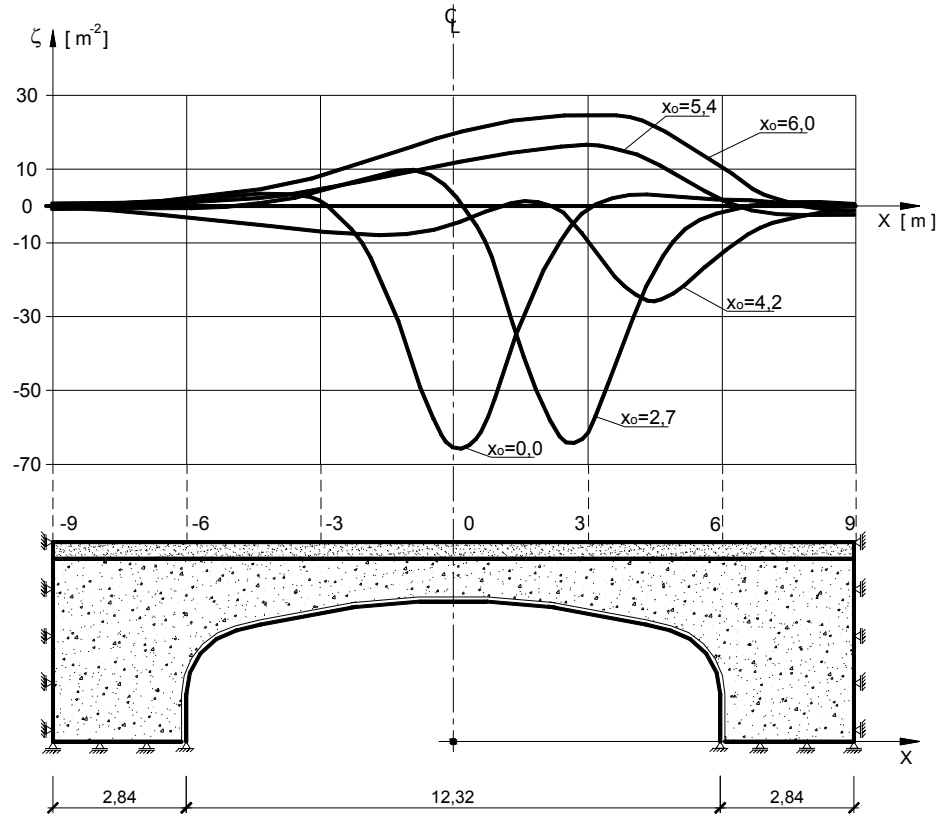

Fig. 19. Longitudinal profiles of the influence surfaces
(at the top of a steel corrugated plate, $y_0 = 0.76$ m)

The transverse profiles of the influence surface of normal stresses σ_x are smooth, similar to the curves representing deflections under concentrated force (for the sake of comparison the curves presented in figure 6 concern the result of loading in the form of two row of vehicle's wheel positioned along the bridge axis). In figure 21, there are shown the same results, but for the bottom edge of the strip analysed. Those curves testify to a decisive influence of axial forces on normal stress in the circumferential strip, which can be seen in figures 11 and 12 showing the results of in-situ monitoring tests.

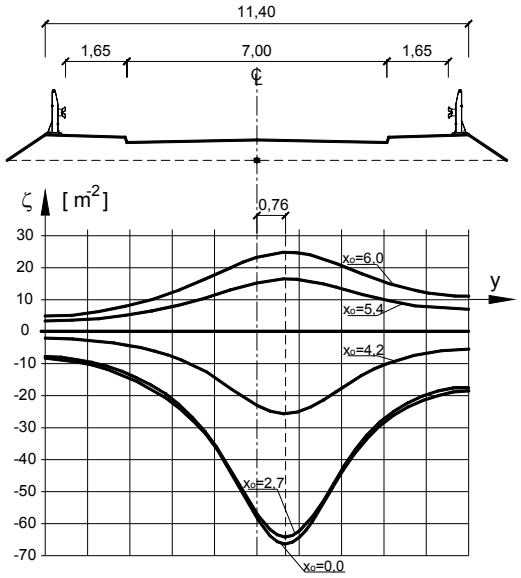

Fig. 20. Transverse profiles of the influence surfaces (at the top of a steel corrugated plate, $y_0 = 0.76$ m)

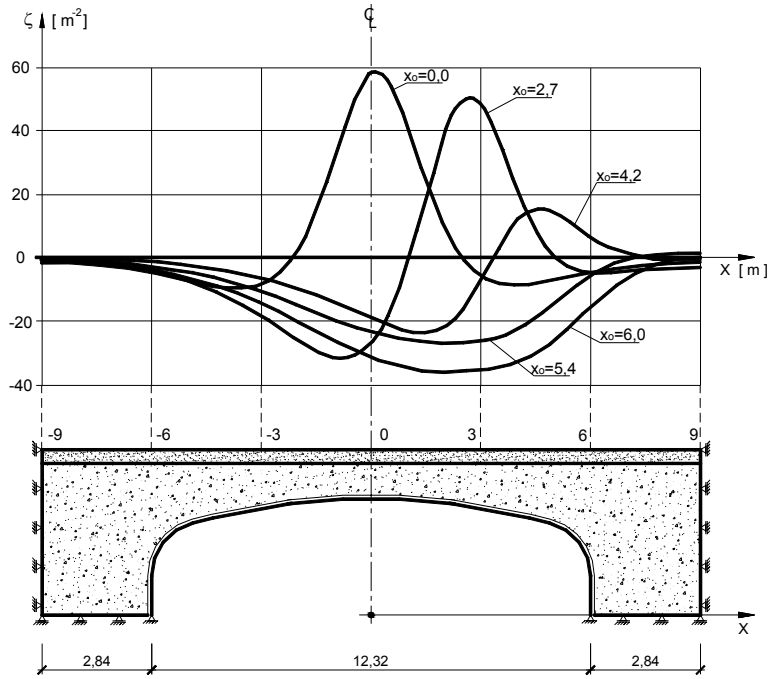

Fig. 21. Longitudinal profiles of the influence surfaces (at the bottom of a steel corrugated plate, $y_0 = 0.76$ m)

5. SUMMARY

A comparison of current measurement results with the results of measurements just after completion of construction [4] (about the twenty eight-month span) provides the basis for a general conclusion that consolidation of soil backfill due to service loads leads to a substantial increase in a global stiffness of construction. It is seen as a significant reduction of both deflection and unit strains (normal stresses). This phenomenon of the structure adaptation to the loading is still observed after two-year period of bridge service. This can suggest that the process of structure adaptation has not been completed (or it is likely to be disappearing but as a long-term effect). This is a very specific feature of soil–steel structures [10].

Under a short-term (live) load the structure shows an elastic behaviour. The measurement of deflections provides evidence that a direct deformation of loaded structure occurs. This results in the comparatively small values of displacements which still remain after the load removal, as can be seen in the case of the typical, reinforced or pre-stressed concrete bridges. For that reason, in the calculation, one can apply a classical linearly elastic formulation of FEM, i.e. the method of internal forces analysis presented in this work. The numerical results obtained from this model show a very limited utilization of the strength of steel shell subject to live load.

In the case of measurement of unit strains, a specific structural work of soil–steel structure in the form of interaction between shell and soil-backfill is noticeable in a tangent plane of the contact layer. The scope of the analysis covers the assessment of shell behaviour subject to live loads in terms of statics, i.e. the assessment of momentary effect. In order to apply the above conclusions to a larger group of the structures of this type, a numerical analysis presented in [4], [10] is required.

REFERENCES

[1] ABDEL-SAYED G., BAKHT B., *Soil–steel structure design by the Ontario Code.* Part 2. *Structural consideration*, Canadian Journal of Civil Engineering, 1981, Vol. 8, No. 3, pp. 331–341.

[2] ABDEL-SAYED G., SALIB S.R., *Minimum depth of soil cover above soil–steel bridges*, Journal of Geotechnical and Geoenvironmental Engineering, 2002, Vol. 128, No. 8, pp. 672–681.

[3] ANTONISZYN G., *Parametric analysis of steel shell embeded in soil* (in Polish), Drogownictwo, 2004, No. 4, pp. 135–139.

[4] BĘBEN D., MAŃKO Z., *Research of road bridge made of steel corrugated plates of Super Cor SC-56B type under static load* (in Polish), I Sympozjum *Diagnostyka i Badania Mostów*, Opole, 4–6 April, 2001, pp. 27–70.

[5] GIRGES Y., ABDEL-SAYED G., *Three-dimensional analysis of soil–steel bridges*, Canadian Journal of Civil Engineering, 1995, Vol. 22, pp. 1155–1163.

[6] HAFEZ H., ABDEL-SAYED G., *Finite element analysis of soil–steel structures*, Canadian Journal of Civil Engineering, 1983, Vol. 10, pp. 287–294.

[7] JANUSZ L., *Application of flexible steel structures, flexible steel and plastic pipes for building culverts, bridges and tunnels* (in Polish), The 1st International Conference *Modern Technologies in Highway Engineering*, Poznań, 10–11 September, 1998, pp. 373–383.

[8] JANUSZ L., *Small bridges made from corrugated steel plates as a fast and cheap alternative to traditional methods of construction of small bridges* (in Polish), IV Krajowa Konferencja Naukowo-Techniczna *Problemy projektowania, budowy i utrzymania mostów małych*, Wrocław, 2–3 December, 1999, pp. 148–155.

[9] LADE P.V., *Elastoplastic stress–strain theory for cohesionless soil*, Journal of Geotechnical Engineering Division, ASCE, 1975, 104(GT2), pp. 193–209.

[10] MACHELSKI CZ., ANTONISZYN G., TOCZKIEWICZ R., *In situ tests of internal forces and displacements of Super Cor bridge along the route of roadway Polanica–Szczytna subject to service load* (in Polish), Raport SPR No. 110/2003, Instytut Inżynierii Lądowej Politechniki Wrocławskiej.

[11] MACHELSKI CZ., ANTONISZYN G., *Internal forces in soil–steel bridge structures* (in Polish), Drogi i Mosty, 2003, No. 2, pp. 33–57.

[12] MACHELSKI CZ., ANTONISZYN G., *Investigation of soil–steel culverts of small structural height* (in Polish), Inżynieria i Budownictwo, 2004, No. 4, pp. 202–205.

[13] MACHELSKI CZ., MICHALSKI B., *Live load deflection on soil–steel bridge* (in Polish), V Krajowa Konferencja Naukowo-Techniczna *Problemy projektowania, budowy oraz utrzymania mostów małych i średnich rozpiętości*, 2–3 December, 2004, Wrocław, pp. 309–316.

[14] MACHELSKI CZ., *The application of kinematic method to determining the influence functions of internal forces in bar structures* (in Polish), Inżynieria i Budownictwo, 1998, No. 7, pp. 372–375.

[15] MIRZA C., BAKHT B., *Soil–steel structure design by the Ontario Code*. Part 1. *General and geotechnical considerations*, Canadian Journal of Civil Engineering, 1981, Vol. 8, No. 3, pp. 317–330.

[16] MOHAMMED H., KENNEDY J.B., *Economical design for long-span soil–metal structures*, Canadian Journal of Civil Engineering, 1996, Vol. 23, pp. 838–849.

[17] MRÓZ Z., PIETRUSZCZAK S., *A constitutive model for sand with anisotropic hardening rule*, Int. Journ. Numerical and Analytical Methods in Geomechanics, 1983, No. 7, pp. 305–320.

[18] Ontario Highway Bridge Design Code –91, 3rd Edition, Ministry of Transportation, 1992.

[19] VASLESTAD J., JANUSZ L., BEDNAREK B., *Corrugated plate structures in bridge engineering* (in Polish), Materiały budowlane, 11'2000 (No. 339), pp. 48–49.

[20] VASLESTAD J., *Long-term behaviour of flexible large-span culverts*, Directorate of Public Roads, Norwegian Road Research Labolatory, Publication No. 74, Oslo, September 1994.

[21] VASLESTAD J., *Soil structure interaction of buried culverts*, Institutt for Geoteknikk, Norges Tekniske Hogskole, Universitetet I Trondheim, 1990.